J. Fluid Mech. (2021), *vol*. 909, R1, doi:10.1017/jfm.2020.992

Acoustic theory of the many-bladed contra-rotating propeller: the event line and the precession of the interaction source

A.B. Parry[1,†] **and M.J. Kingan**[2]

[1]30 Ypres Road, Allestree, Derby DE22 2LZ, UK

[2]Department of Mechanical Engineering, University of Auckland, Auckland 1010, New Zealand

(Received 6 September 2020; revised 28 October 2020; accepted 8 November 2020)

In the asymptotic theory of interaction noise from contra-rotating propellers with many blades, previous work in the frequency domain has shown that, for each combination mode/tone, the critical points that dominate the acoustic radiation can be linked to two criteria (sonic and normal-edge) and to a radial event line that spins around the annulus at the same speed as the mode. Thus the speed is different for each combination tone. In real time, however, the interactions precess around the annulus at a single speed, governed by the 'firing order' of the interactions, with that speed being (in general) considerably different from that of either the front or rear blade rows. The precession of the interaction is described here in detail and then demonstrated by application to three relevant architectures, including a rotor–stator configuration. The paper then considers how the blade leading-edge design affects the radial variation in the interaction location and analyses the interactions from the viewpoint of a far-field observer. The paper also connects previous time- and frequency-domain results by showing that the sonic and normal-edge criteria can be derived in the time domain using the precession speed. The case of equal blade numbers is also included, for which the precession speed becomes infinite but for which, nonetheless, the sonic and normal-edge criteria still apply.

Key words: wakes, aeroacoustics

1. Introduction

There has been an increasing body of work on the use of high-blade-number asymptotic approaches to study propeller noise and, perhaps more importantly, understand the physics underlying the source generation mechanisms. The initial work focused on single-rotating propellers. The far-field radiation can be calculated, numerically, from the analytic

† Email address for correspondence: anthony.parry.pig@gmail.com

'frequency-domain' solutions of Hanson (1983) and Parry (1988). However, these methods involve, for each individual tone, a double integration over the blade planform area (chord and span) in which the integrand includes Bessel functions and complex phase terms. Using a frequency-domain approach, Parry & Crighton (1986, 1989*a*) showed that subsonic propeller noise could be predicted using a simplified formula that removed the need for an integration over the blade span and showed how the noise is dominated by radiation from the blade tips, with the result linked precisely to the tip geometry. Crighton & Parry (1991, 1992) applied the approach to supersonic propellers where the noise is dominated to leading order by radiation from a sonic radius with a lower-order term arising from the blade tips. For both the subsonic and supersonic cases, the asymptotic approach produced closed-form algebraic results in the form of simple algebraic expressions, which were, nonetheless, still accurate and showed how the noise was related to the geometry and aerodynamics of a particular propeller radius.

In a novel time-domain analysis of the thickness noise of supersonic single-rotating propellers, Amiet (1988) showed that the sound radiated to the far field was dominated by regions of the blade that satisfied two criteria. First, that the Mach number of the blade at that location was precisely unity when resolved in the direction of the observer and, second, that the leading edge of the propeller blade was normal to a line drawn between it and the observer. We will refer to these criteria as the 'sonic' and 'normal-edge' conditions, respectively. Amiet argued that a time-domain analysis, rather than a frequency-domain approach, was essential to properly understand the underlying physics and to obtain the dominant source locations. Parry (1995) showed that Amiet's criteria could be obtained in the frequency domain. For other work on asymptotic analyses of single-rotating propeller noise, we refer the reader to the discussions in Kingan & Parry (2019) and Parry & Kingan (2019).

There has been little work on the application of asymptotic analyses to contra-rotating propellers. From the numerical point of view, Envia (2015) extended previous work on single-rotating propellers to the contra-rotating case, with the radiation expressions, as before, requiring a high-fidelity calculation of the local source region. For analytical and/or semi-numerical approaches, Kingan & Parry (2019) used the framework provided by the frequency-domain description of Hanson (1985), Parry (1988, 1997) and Parry & Crighton (1989*b*), regarding convected wake interactions, and extended the two-dimensional surface asymptotic approach of Parry (1995) to contra-rotating propellers, including the effects of blade sweep, quasi-three-dimensional blade unsteady response and sub- or supercritical wake–blade interactions. The analyses once again produced simplified, largely algebraic, results and showed that the noise is dominated in most cases by localised critical points on the surface of revolution described by the rear blade leading edges. In certain cases – dependent on blade sweep and the order of the circumferential spinning mode – radial or azimuthal one-dimensional continuums of critical points can be present or, exceptionally, a two-dimensional continuum of critical points.

Kingan & Parry (2019) validated their asymptotic approach extensively by comparing their results with full numerical calculations – of a real engineering test case – over a range of combination frequencies and azimuthal modes, including the zero-mode case, and for both straight and swept propeller blades. For all cases, there was good agreement between the asymptotic results and the numerical calculations (that had, themselves, been validated via many previous comparisons with a wide range of experimental data), showing that the asymptotics could be applied to prediction and design (see Kingan & Parry, 2020*a*).

Parry & Kingan (2019) explored the underlying physics and showed that, in the frequency domain, the locations of the interaction sources for each combination tone can be described by an 'event line' – where the phrase 'event' was taken from the paper of

Tyler & Sofrin (1962) on rotor–stator interaction – which represents the source locations at a fixed reception time and spins around the annulus at the speed of the acoustic mode (associated with the combination tone). Parry & Kingan (2019) explained that, at the critical source locations, this event line has a resolved Mach number of unity in the direction of the far-field observer and is normal to a line drawn between it and the observer, i.e. the event line (for each individual combination tone) satisfies the two criteria of Amiet (1988). Indeed, perhaps surprisingly, Parry & Kingan (2019) showed that the two criteria are still satisfied even when the relevant acoustic mode number is zero and the event line spins around the annulus at infinite speed.

Regarding analytical work on contra-rotating propeller noise in the time domain, the authors are aware only of the work of Kingan & Parry (2020*b*), who considered the interactions between convected wakes from the front propeller and a blade of the rear contra-rotating row. Kingan & Parry (2020*b*) hypothesised that the sharp peaks in the radiated acoustic waveform would be significantly enhanced when the reception time, for a particular wake–blade interaction, became stationary in terms of radius. They showed that, at such a radius, the local trace velocity was precisely sonic when resolved in the direction of the observer.

Here, our aim is to understand the physics of convected wake interactions on contra-rotating propellers in the time domain, rather than just for individual frequencies. In particular, we focus on the location and motion of the interaction 'events' as a function of time and space, both radially and circumferentially. We emphasise that the analytical framework for contra-rotating propeller noise that underpins the analysis – namely that of Hanson (1985), Parry (1988, 1997) and Parry & Crighton (1989*b*) – has been well validated against a range of experimental data. Nonetheless, from the point of view of steady and unsteady aerodynamics, it is important to point out that the general approach neglects a number of effects such as the presence of swirling or radial flow between the two blade rows, the mutual interference that occurs between the vortical and potential fields generated by the front and rear blade rows, the end effects (at the hub and tip) that contribute to the unsteady response, and the thickness and camber of the blades. Most of these effects could be included through extensions to the approach. Despite these limitations, there are detailed discussions of the experimental validation cases in Kingan & Parry (2019) as well as of validation of the asymptotic approach via comparisons with full numerical calculations. To demonstrate the accuracy of the asymptotic (or many-bladed) approach, one of the comparisons from that paper is shown here, in figure 1, for the first interaction tone produced by a contra-rotating propeller with front and rear blade numbers of 12 and 9, respectively.

The paper is laid out as follows. In § 2 we present the three-dimensional coordinate system and the aerodynamic and acoustic parameters. The locations of the convected wake interactions are discussed in § 3 in terms of the 'firing order' as a function of time and circumferential location; examples are discussed for various blade number combinations and architectures; then, we analyse the variation in interaction location with radius. In § 4 the interactions are discussed relative to a far-field observer.

2. Coordinate system

In order to allow comparison with the results of Kingan & Parry (2019, 2020*a*,*b*) and Parry & Kingan (2019) we will use their notation where possible, though we will define the parameters here explicitly because of some differences between the frequency-domain and time-domain publications. The architecture involves two rotating frames, and one absolute frame, as well as important reference points such as the front rotor wake, the

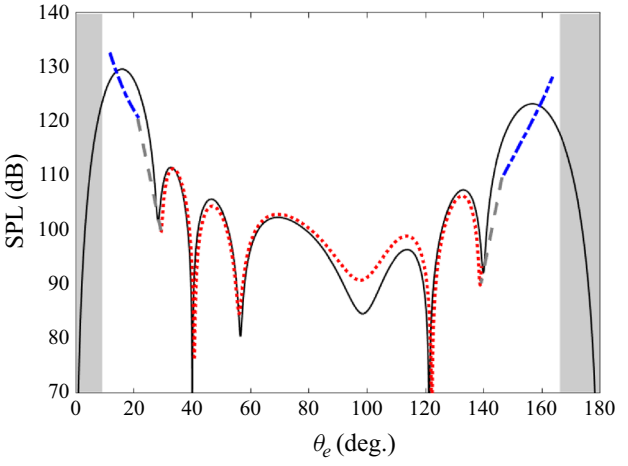

Figure 1. Plot of sound pressure level (SPL) versus θ for the first interaction tone. The solid black line denotes numerical solutions whilst interior stationary point solutions are denoted by the blue dash-dotted lines and boundary critical point solutions are denoted by the red dotted line. The shaded regions correspond to locations where no critical points exist, and the grey dashed lines denote interpolated levels within the exclusion zones. (From Kingan & Parry, 2019.).

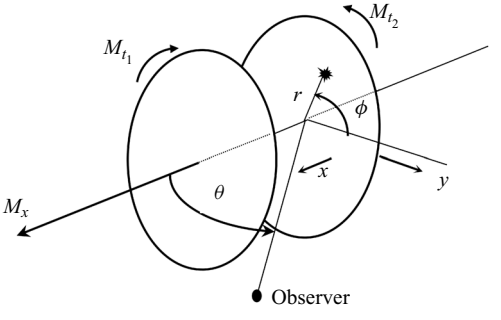

Figure 2. Propeller coordinate system.

rear blade leading edge and the two propeller pitch change axes, and it will be necessary to use all of these frames and locations. The analysis uses a cylindrical coordinate system, (x, r, ϕ), where x is the axial coordinate, which is parallel to the propeller axis, r is the radial coordinate and ϕ is the azimuthal angle. The coordinate system is shown in figure 2. Subscripts 1 and 2 denote parameters associated with the upstream and downstream rotors, respectively, and subscripts x, t and r are used for the Mach numbers in the axial, rotational (at the tip radius) and helical (at radius r) directions, respectively. In particular, the rotors move with Mach number M_x in the positive x direction; the upstream and downstream rotors rotate in the negative and positive ϕ directions with tip rotational Mach numbers M_{t_1} and M_{t_2}, respectively.

The effect of the flow induced by the rotors is neglected (which is entirely in keeping with the helicoidal surface theory of Hanson (1983)) so that the stagger angle, α_i, $i = 1, 2$, of each blade is defined by $\tan\alpha_i = rM_{t_i}/M_x$ and, for each row, $M_{r_i} = \sqrt{M_x^2 + r^2M_{t_i}^2}$ is the section relative, or helicoidal, Mach number. The propeller blades have leading-edge sweep $s(r)$ measured from the pitch change axis and each propeller has B_i blades with front

and rear pitch change axes separated by a distance g in the axial direction. The observer lies in the $\phi = 0$ plane at polar angle θ from the x axis. For convenience, distances have been normalised on the tip radius R, velocities on the speed of sound c_0 and time on R/c_0. The hub radius is r_h. For a contra-rotating propeller, the radiated tones can be described as a double Fourier series of combination tones (n_1, n_2) at frequencies $\eta = n_1 B_1 M_{t_1} + n_2 B_2 M_{t_2}$ and with azimuthal order $\nu = n_2 B_2 - n_1 B_1$. Source time is denoted by τ and the specific times at which the wake centreline of the front reference blade interacts with the rear reference blade are given by τ_0 where, in the general case of swept blades, $\tau_0 = \tau_0(r)$. We suppose that the pitch change axis of the rear row reference blade lies at $\phi = 0$ when $\tau = 0$. It is also convenient to introduce the term $S(r) = s(r)/M_{r_2}(r)$.

3. Physics of the interaction in the time domain

3.1. *Precession of the interaction*

In this section we consider the interactions between specific blades on the rear rows and the wakes from specific blades of the front row. Here, an interaction occurs when the centreline of the wake from an upstream blade impinges on the leading edge of a downstream blade. In reality, of course, since the wake and blade leading edge are of finite thickness, this interaction occurs over a finite time. Tyler & Sofrin (1962) refer to these interactions as blade–vane events or, more simply, just as 'events'. In the general case, the wakes from the front propeller do not all interact simultaneously with the rear propeller blades for the simple reason that the number of wakes, B_1, is not the same as the number of blades, B_2, on the rear row. In the time domain, the interactions can be viewed as occurring at locations that 'jump' around the circumference, sometimes by considerable distances. For rotor–stator interactions, Tyler & Sofrin (1962) referred to this effect as the 'firing order'. Here we will suppose that this sequence of events represents the precession of the interaction around the circumference and consider it in detail.

In order to determine the speed at which the individual interactions precess around the circumference, we start by assuming that, in figure 3, the blades are numbered in the positive ϕ direction on each row and that the interaction between blade 0 on the front row and blade 0 on the rear row occurs at source time $\tau = 0$. For the purposes of the analysis that follows, we assume that the blade numbers B_1 and B_2 are relatively prime. If B_1 and B_2 have a common factor then there will be more than one interaction occurring simultaneously and the analysis applies over an appropriate subsection of the annulus, with the results then repeating over each subsection. Of course, the blades chosen as the zeroth blades on each row are arbitrary. The pitch is given by $P_1 = 2\pi r/B_1$ and $P_2 = 2\pi r/B_2$ on the front and rear row, respectively, so that the azimuthal gap between blade j_1 on the front row and blade j_2 on the rear row is

$$\Delta\phi_{j_1,j_2} = j_1 \frac{P_1}{r} - j_2 \frac{P_2}{r} = 2\pi \frac{(j_1 B_2 - j_2 B_1)}{B_1 B_2}. \tag{3.1}$$

As, with our normalisation, the relative angular speed is $(M_{t_1} + M_{t_2})$, the time it takes from the interaction between the datum blades to that of the interaction between blade j_1 on the front row and blade j_2 on the rear row is

$$\Delta\tau_{j_1,j_2} = \frac{\Delta\phi_{j_1,j_2}}{(M_{t_1} + M_{t_2})} = \frac{2\pi(j_1 B_2 - j_2 B_1)}{B_1 B_2 (M_{t_1} + M_{t_2})}. \tag{3.2}$$

In that time, the interaction has moved from $\phi_2 = 0$ to $\phi_2 = 2\pi j_2/B_2$, where $\phi_2 = \phi - M_{t_2}\tau$ is the azimuthal angle in the frame of reference of the rear row, so we can deduce that

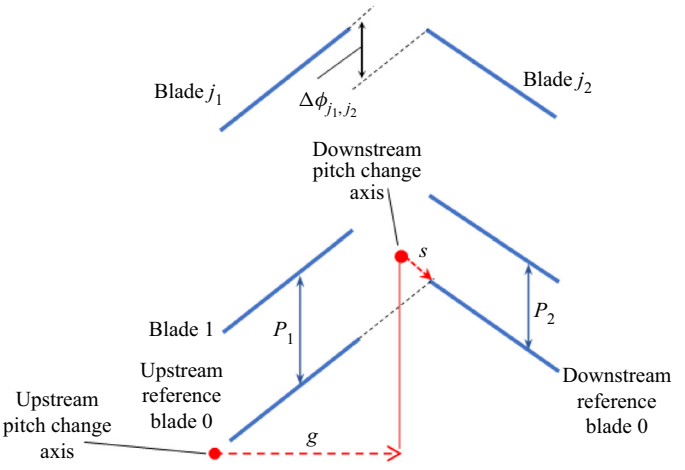

Figure 3. Two-dimensional cascade definition.

the effective speed with which the interaction has moved in the absolute frame is $M_{j_1,j_2} = M_{t_2} + (2\pi j_2/B_2\Delta\tau_{j_1,j_2})$. Then, after using (3.2), we obtain the effective interaction speed and interaction location as

$$M_{j_1,j_2} = \frac{j_2B_1M_{t_1} + j_1B_2M_{t_2}}{j_1B_2 - j_2B_1}, \quad \phi_{j_1,j_2} = \frac{2\pi(j_2B_1M_{t_1} + j_1B_2M_{t_2})}{B_1B_2(M_{t_1} + M_{t_2})}. \tag{3.3a,b}$$

The result for interaction speed in (3.3*a*,*b*) is very familiar and, suitably normalised, looks like the standard relationship for circumferential mode-phase speed η/ν in turbomachinery (see e.g. Tyler & Sofrin, 1962) in terms of an angular frequency $\eta = n_1B_1M_{t_1} + n_2B_2M_{t_2}$ and mode number $\nu = n_2B_2 - n_1B_1$. However, the standard relationship applies to the frequency domain and to a range of different combination tones (n_1, n_2) each of which has its own frequency and azimuthal order so that every one rotates at a different speed. Here it is important to realise that (3.3*a*,*b*) is a time-domain result and that (j_1, j_2) is used to refer to interactions between specific blades with the fixed values j_1 and j_2 being determined by the blade numbers. In order to determine which interactions occur in which order, it follows from (3.1) and (3.2) that, after the 0–0 front and rear blades interact, the next interaction occurs a short time $\Delta\tau$ later where

$$\Delta\tau = \frac{2\pi}{B_1B_2(M_{t_1} + M_{t_2})} \times \min_{\substack{0\le j_1\le B_1-1\\ 0\le j_2\le B_2-1\\ j_1B_2-j_2B_1>0}} \{j_1B_2 - j_2B_1\}, \tag{3.4}$$

so that $\Delta\tau$ is the time taken between successive wake interactions (and it is important to note that those interactions do not necessarily occur between adjacent blades). The values (j_1, j_2) that are obtained as the solution to (3.4) are related to the blade numbers B_1 and B_2 and can be treated as fixed for that blade number combination.

By considering the blade row speeds and blade spacings, and using a little simple arithmetic, it is easy to show that the next interaction will occur between blades $(2j_1, 2j_2)$ at azimuthal location $\phi_{2j_1,2j_2} = 4\pi(j_2B_1M_{t_1} + j_1B_2M_{t_2})/[B_1B_2(M_{t_1} + M_{t_2})]$, and so on, so that the effective speed at which the interaction location moves – or precesses – is continuous around the annulus. If we suppose that l and m are the values of j_1 and j_2 that

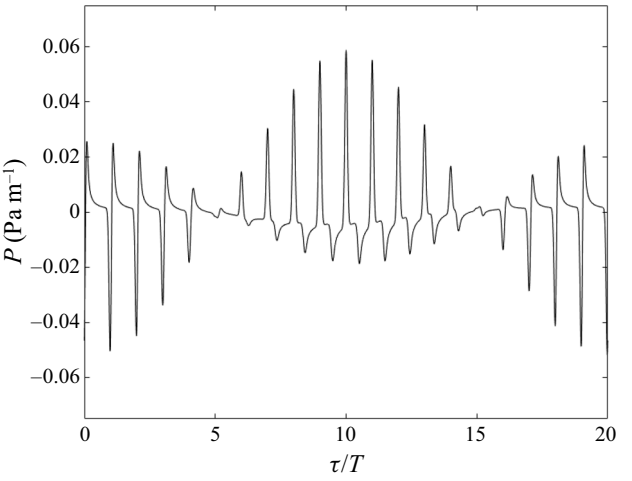

Figure 4. The pressure field radiated from $r = 0.7$ for a straight propeller, plotted in terms of leading-edge source time τ.

are required in (3.4), then the speed (or tip Mach number) at which the interaction events precess around the annulus is

$$M_p = \frac{mB_1M_{t_1} + lB_2M_{t_2}}{lB_2 - mB_1}. \tag{3.5}$$

In practice, the interactions are discrete but the idea that the interactions are moving continuously becomes more acceptable for higher blade numbers. Indeed, the assumption of a continuum of interactions is completely consistent with the many-bladed asymptotic approach, used in the frequency-domain analyses of Kingan & Parry (2019, 2020*a*) and Parry & Kingan (2019), in which the blade numbers $B_1 \to \infty$, $B_2 \to \infty$ because then the time interval between interactions $\Delta\tau \to 0$.

3.2. *Examples*

We will consider a few simple examples to illustrate the values of l and m. Note first, though, that the integers l and m can be negative, where negative values are obtained if the blades are counted in the opposite (or negative ϕ) direction, provided that we still maintain $lB_2 - mB_1 > 0$ to ensure that we are moving forwards in time. Of course, the interactions occur in the same 'firing order' in both forward and reverse cases; the point is that the interaction disturbances can merely be viewed as moving in either the positive or negative direction.

First, we examine the contra-rotating propeller studied by Kingan & Parry (2020*b*) in their time-domain analysis. The propeller had 10 blades on the front row and a single blade on the rear row, and tip rotational Mach numbers $M_{t_1} = M_{t_2} = 0.7$. That case is straightforward, as all the interactions (events) must occur at the leading edge of the same rear blade so that $m = 0$; the interactions must also be caused by the wakes from successive blades on the front row so that $l = 1$ and $M_p = M_{t_2}$. We emphasise that the interactions are not continuous; from (3.4) they occur discretely at source time intervals of $\Delta\tau = 2\pi/B_1(M_{t_1} + M_{t_2}) = \pi/7$, given as the period T by Kingan & Parry (2020*b*). In order to demonstrate the effect of the source we show, in figure 4, a full numerical calculation for this contra-rotating propeller, in the time domain, with the pressure per unit span, P,

radiated from the mid-span ($r = 0.7$) of the blade. Figure 4 has been recalculated and is plotted here in terms of (leading-edge) source time τ rather than reception time t (as it was in figure 5(a) of Kingan & Parry (2020*b*)). The source period is normalised on T so that pulses occur at multiples of $\tau/T = 1$, precisely as expected. The calculation also serves to demonstrate the sharpness of the interaction impulses in a practical wake–blade interaction case. For this configuration, the interactions can be considered to be rotating with the rear blade leading edge and at the speed of the rear blade row.

Second, we consider the examples used by Kingan & Parry (2019) in demonstrating the accuracy of their asymptotic, frequency-domain analysis of contra-rotating propellers. Whilst their example architectures had different degrees of sweep, they all had 12 blades on the front row and 9 blades on the rear row. In a fixed reference frame, the front blades are thus 30° apart and the rear blades are 40° apart. Assuming that the zeroth front and rear blades are aligned at $\tau = 0$ then, taking into account the direction of motion of the two blade rows, a little arithmetic can be used to show that the next interaction will occur between the third blade of the front row and the second blade of the rear row. (Of course, since for this case there is a common factor of 3 in the blade numbers, the interactions repeat spatially every 120°.) The relevant values are thus $l = 3$ and $m = 2$, and we obtain the precession speed of $M_p = 8M_{t_1} + 9M_{t_2}$ (which is much faster than that of the case with a single-bladed rear row) and the time interval of $\Delta\tau = 2\pi/36(M_{t_1} + M_{t_2})$ between interaction events. By counting blades in the opposite direction, an alternative solution is also obtained with $l = -1$ and $m = -1$ for which the interactions precess in the reverse direction at $M_p = -(4M_{t_1} + 3M_{t_2})$, which is less than half that of the precession speed in the forward (or positive ϕ) direction. The interval between interaction events is the same as that of the forward propagating sequence of interactions.

Purely for completeness, we will also consider a third case relating to a rotor–stator interaction. For such architectures, the stator numbers are usually selected to be more than twice the number of rotors in order to ensure the first interaction tone cannot propagate. We thus pick the numbers $B_1 = 18$ and $B_2 = 40$. In a fixed reference frame, the rotors are thus 20° apart and the stators are 9° apart. Once again, we assume that the zeroth front and rear blades are aligned at $\tau = 0$. The next interaction is then easily shown to occur between the fifth blade of the front row and the eleventh blade of the rear row. (Of course, since for this case there is a common factor of 2 in the blade numbers, the interactions repeat spatially every 180°.) The relevant values are thus $l = 5$ and $m = 11$, and we obtain the precession speed of $M_p = 220M_{t_1}$ and the time interval of $\Delta\tau = 2\pi/360M_{t_1}$ between interaction events. Alternatively, we can use $l = -4$ and $m = -9$ and obtain $M_p = -81M_{t_1}$ and the same value of $\Delta\tau$.

3.3. *Interaction location as a function of radius*

The analysis of Kingan & Parry (2020*b*) showed that the front and rear reference blades, on a contra-rotating propeller, interact at source times that vary across the blade span due to the effect of blade sweep. Their derivation (given as (2.11) in Kingan & Parry (2020*b*)) is straightforward, as it is based solely on blade geometry and speed. With our normalised parameters and definition of $\tau = 0$, the expression simplifies and the reference blade interaction source times are $\tau_0(r) = S(r)$, where both τ_0 and S are zero at the hub: $r = r_h$.

The precession speed is given by (3.5), so that the azimuthal location at which the interactions take place can be expressed as $\phi_{ev} = M_p(\tau - \tau_0)$, where we have used the subscript 'ev' to reflect the fact that the wake–blade interactions are referred to by

Tyler & Sofrin (1962) as 'events'. We will require the radial derivative of ϕ_{ev} in the following section and we get

$$\frac{\mathrm{d}\phi_{ev}}{\mathrm{d}r} = -M_p S'(r). \tag{3.6}$$

4. Interactions as viewed by the observer

For the observer-based analysis, we follow much of the approach given in § 4 of Parry & Kingan (2019) except, crucially, for the fact that the Mach number of the interaction disturbance, or event, is dependent not on the front and rear propeller blade Fourier harmonics (n_1, n_2) but on a precession speed that is fixed for a given propeller architecture and is given here by (3.5). As the propeller is advancing with Mach number M_x, and the disturbance rotates (or precesses) around the annulus with Mach number M_p, the combined Mach number M_{obs} of an 'event' at radius r towards an observer in the far field at polar angle θ can be obtained, using simple geometry, as $M_{obs} = M_x \cos\theta - \mathbb{M}$, where $\mathbb{M} = rM_p \sin\theta \sin\phi_{ev}$ is the resolved component of the rotating disturbance's precession speed towards the observer. The combined speed of the disturbance, in the direction of the observer, is thus sonic when $\mathbb{M} = -(1 - M_x \cos\theta)$ or

$$\sin\phi_{ev} = -\frac{(1 - M_x \cos\theta)}{rM_p \sin\theta}. \tag{4.1}$$

The location of an interaction event, at the leading edge of a propeller blade, is given by

$$x_{ev} = -M_x S + M_x \tau, \quad y_{ev} = r\cos\phi_{ev}, \tag{4.2a,b}$$

where x and y are Cartesian coordinates in the horizontal plane in figure 2. For an observer in the far field, the dot product of the tangent vector to the event line with the position vector of the event location, relative to the observer, is given by

$$\ell = \frac{\mathrm{d}x_{ev}}{\mathrm{d}r}\cos\theta + \frac{\mathrm{d}y_{ev}}{\mathrm{d}r}\sin\theta, \tag{4.3}$$

and we find, after differentiating (4.2*a*,*b*) with respect to the radius r, and also using (3.6) and (4.1), that $\ell = 0$, and the event line is normal to the line between it and the far-field observer, when

$$\frac{\sin\theta\cos\phi_{ev}}{\mathrm{d}S/\mathrm{d}r} = 1. \tag{4.4}$$

In their time-domain analysis, Kingan & Parry (2020*b*) (see (4.6) and (4.7) and the accompanying discussion therein) showed that the term on the left-hand side of (4.4) represented the Mach number of the wake centreline/leading-edge impingement point (or trace Mach number along the reference blade's leading edge) resolved in the direction of the observer. (They used a fixed coordinate system so their Mach number was defined relative to the fluid. That is not the case here.) For a swept blade, the Kingan & Parry (2020*b*) analysis showed, further, that the condition (4.4) – representing a trace Mach number of unity towards the observer – occurred when the reception times were stationary with respect to the radius r and, as a consequence, it coincided with an enhanced accumulation of noise from across the blade span and to strong peaks in the resultant noise waveform received by the observer. In the time domain, therefore, (4.4) can be viewed as a condition, or requirement, for enhanced peaks in the radiated sound field.

We have thus shown that this enhanced noise radiation in the time domain corresponds, not just to a wake/blade leading-edge trace Mach number of unity, resolved in the direction

of the observer, but also to the criteria of Amiet (1988), which relate to the shape and motion of the disturbance event line that precesses around the circumference. The first of these criteria is the sonic condition, in which the disturbance moves at a Mach number of unity in the direction of the observer. Note that this Mach number relates to that of the event line and not of the impingement point along the reference blade's leading edge. The second criterion is the normal-edge condition, in which the tangent to the event line is normal to a line drawn between it and the observer.

For the case in which the two blade rows have equal numbers ($B_1 = B_2$), the interactions occur simultaneously at all the rear blade leading-edge locations. To understand this case, we must proceed with care and consider the limit as the two blade numbers approach each other. Formally, at each radial station, we consider the interactions between two cascades translating in opposite directions with speeds M_{t_1} and M_{t_2}. This approach is completely in keeping with that taken in the strip-theory model used for aerodynamic interactions by Parry & Crighton (1989*b*), Parry (1997) and Kingan & Parry (2019, 2020*a*,*b*). Specifically, we suppose that the cascade pitches are $P_1 = P + \delta P$, $P_2 = P$ and $P = O(B^{-1})$, with $\delta P = O(B^{-2})$, $B \to \infty$. (Here we have specified the magnitude of δP for definiteness but, in fact, we merely require $\delta P = o(B^{-1})$.) Then, we find that $l = m = 1$ and, as might be expected, the precession speed $M_p = (M_{t_1} + M_{t_2})P/\delta P \to \infty$ as $\delta P \to 0$ (or $B \to \infty$). Despite the fact that the precession speed is infinite, we also find from (4.1) that, provided the observer is not positioned on the propeller axis (i.e. $\theta \neq 0$), the sonic condition is still satisfied when $\phi_{ev} = 0, \pi$ (and the event line passes through the x–y plane) and, from (4.4), that the normal-edge condition is then satisfied at observer locations $\theta = \pm \sin^{-1} \mathrm{d}S/\mathrm{d}r$. When the observer is positioned on the propeller axis ($\theta = 0$), ϕ_{ev} is indeterminate and we thus find that the two criteria are satisfied at all azimuthal locations provided that $\mathrm{d}S/\mathrm{d}r = 0$. For swept propellers, the enhanced noise thus comes from locations distributed around a ring (or rings), at a radius (or radii) satisfying $\mathrm{d}S/\mathrm{d}r = 0$ and, for straight propellers (for which $\mathrm{d}S/\mathrm{d}r = 0$ everywhere), it comes from the entire nominal propeller disk. These time-domain results echo completely those found in the frequency domain by Parry & Kingan (2019) for the zero mode case.

5. Conclusions

This paper has discussed the location of convected-wake interactions on a contra-rotating propeller in real time. In the general case, these interactions occur at discrete, and equal, time intervals at different locations around the circumference. However, as the blade numbers tend to infinity, the process tends to a continuum of interactions. In this limit, we showed how the interaction location precesses around the circumference at a speed different from that of the front or rear blades and given by a combination of the two blade numbers and the two tip speeds. The relevance of the calculation has been demonstrated by application to recent frequency- and time-domain work on contra-rotating propellers and also to a rotor–stator type configuration. We have exploited previous time-domain work on the radial variation in the location of the wake interactions on contra-rotating propellers to produce a complete (radial and azimuthal) space–time expression for the interaction location. The radial variation in this location can be considered as a time-domain version of an event line. An analysis from the viewpoint of a far-field observer showed that the sonic and normal-edge conditions are satisfied by the time-domain event line at locations in the nominal propeller disk corresponding precisely to those found in the far field, by Kingan & Parry (2020*b*), to have stationary reception times relative to the radius r and, thereby, to produce enhanced peaks in the radiated waveform.

The paper thus shows that, for a contra-rotating propeller in the time domain, as well as the frequency domain, the dominant noise generation regions are given, once again, by the sonic and normal-edge criteria. Those criteria were first discovered by Amiet (1988) in a time-domain analysis of the thickness noise from a single-rotating propeller. There the criteria applied along the line defined by the propeller's leading edge. We have shown the criteria apply equally well to wake interactions on a contra-rotating propeller – provided that the source line can be suitably defined. That line is the time-domain event line which spins around the annulus at a speed given by the precession speed of the interactions.

Throughout, our aim has been to ensure that the time-domain and frequency-domain analyses are completely consistent and that the physics underlying the noise generation are fully understood, particularly in relation to the dominant source locations.

Declaration of interests. The authors report no conflict of interest.

Author ORCIDs.
A.B. Parry http://orcid.org/0000-0002-4481-2065;
M.J. Kingan http://orcid.org/0000-0003-4265-5307.

References

Amiet, R.K. 1988 Thickness noise of a propeller and its relation to blade sweep. *J. Fluid Mech.* **192**, 535–560.
Crighton, D.G. & Parry, A.B. 1991 Asymptotic theory of propeller noise II: supersonic single-rotation propeller. *AIAA J.* **29**, 2031–2037.
Crighton, D.G. & Parry, A.B. 1992 Higher approximations in the asymptotic theory of propeller noise. *AIAA J.* **30**, 3023–3039.
Envia, E. 2015 Aeroacoustic analysis of a high-speed open rotor. *Intl J. Aeroacoust.* **14** (3 and 4), 569–606.
Hanson, D.B. 1983 Helicoidal surface theory for propeller aerodynamics and noise. *AIAA J.* **21**, 881–889.
Hanson, D.B. 1985 Noise of counter-rotation propellers. *J. Aircraft* **22**, 609–617.
Kingan, M.J. & Parry, A.B. 2019 Acoustic theory of the many-bladed contra-rotating propeller: analysis of the effects of blade sweep on wake interaction noise. *J. Fluid Mech.* **868**, 385–427.
Kingan, M.J. & Parry, A.B. 2020*a* Acoustic theory of the many-bladed contra-rotating propeller: the effects of sweep on noise enhancement and reduction. *J. Sound Vib.* **468**, 115089.
Kingan, M.J. & Parry, A.B. 2020*b* Time domain analysis of contra-rotating propeller noise: wake interaction with a downstream propeller blade. *J. Fluid Mech.* **901**, A21.
Parry, A.B. 1988 Theoretical prediction of counter-rotating propeller noise. PhD thesis, Department of Applied Mathematical Studies, University of Leeds.
Parry, A.B. 1995 The effect of blade sweep on the reduction and enhancement of supersonic propeller noise. *J. Fluid Mech.* **293**, 181–206.
Parry, A.B. 1997 Modular prediction scheme for blade row interaction noise. *J. Propul. Power* **13**, 334–341.
Parry, A.B. & Crighton, D.G. 1986 Theoretical prediction of single-rotation propeller noise. In *10th AIAA Aeroacoustics Conference, Seattle, WA, Jul 9-11. AIAA Paper* 86-1891.
Parry, A.B. & Crighton, D.G. 1989*a* Asymptotic theory of propeller noise. I – subsonic single-rotation propeller. *AIAA J.* **27**, 1184–1190.
Parry, A.B. & Crighton, D.G. 1989*b* Prediction of counter-rotation propeller noise. In *12th AIAA Aeroacoustics Conference, San Antonio, TX, Apr 10-12. AIAA Paper* 89-1141.
Parry, A.B. & Kingan, M.J. 2019 Acoustic theory of the many-bladed contra-rotating propeller: physics of the wake interaction noise critical sources. *J. Fluid Mech.* **880**, 385–427.
Tyler, J.M. & Sofrin, T.G. 1962 Axial flow compressor noise studies. *SAE Trans.* **70**, 309–332.